

Decadal Persistence of Cycles in Lava Lake Motion at Erebus Volcano, Antarctica

Nial Peters^{a,*}, Clive Oppenheimer^a, Philip Kyle^b, Nick Kingsbury^c

^a*Department of Geography, University of Cambridge, Downing Place, Cambridge, CB2 3EN, UK*

^b*New Mexico Institute of Mining and Technology, Socorro, USA*

^c*Department of Engineering, University of Cambridge, Trumpington Street, Cambridge, CB2 1PZ, UK*

Abstract

Studies of Erebus volcano's active lava lake have shown that many of its observable properties (gas composition, surface motion and radiant heat) exhibit cyclic behaviour with a period of ~ 10 min. We investigate the multi-year progression of the cycles in surface motion of the lake using an extended (but intermittent) dataset of thermal infrared images collected by the Mount Erebus Volcano Observatory between 2004 and 2011. Cycles with a period of between $\sim 4-15$ min are found to be a persistent feature of the lake's behaviour and no obvious long-term change is observed despite variations in lake level and surface area. The times at which gas bubbles arrive at the lake's surface are found to be random with respect to the phase of the motion cycles, drawing us to the conclusion that the behaviour of the lake is governed by magma exchange rather than an intermittent flux of gases from the underlying magma reservoir.

*Corresponding author

Email address: `njp39@cam.ac.uk` (Nial Peters)

Keywords: lava lake, thermal imaging, convection, bidirectional flow, conduit

1. Introduction

Persistently active lava lakes are a spectacular but rare form of open-vent volcanism found at only a handful of volcanoes around the world. An active lava lake is the exposed top of a volcano's magmatic plumbing system. Longevity of the lake has been argued to reflect either effective transfer of magma between the lake and the deeper system (e.g. Oppenheimer et al. (2004); Francis et al. (1993)), or a supply of gas bubbles from depth (Witham and Llewelin, 2006; Bouche et al., 2010). This link with the deeper magmatic system makes the study of active lava lakes (sensu Tilling (1987)) of particular importance. It can be shown experimentally that processes occurring at depth will manifest themselves at the surface as changes in the lake's behaviour, for example its surface level (Witham et al., 2006) or gas flux (Divoux et al., 2009). It follows therefore, that observations of lake properties can yield valuable insights into the processes occurring at depth in the magmatic system, where direct measurements are not possible.

Erebus is a 3794 m high stratovolcano located on Ross Island, Antarctica. It is the southernmost active volcano in the world and is known to have hosted an active phonolite lava lake since at least 1972 (Giggenbach et al., 1973). Although other small lakes have appeared intermittently over this period, the main, "Ray" lake, has been a permanent feature of the crater throughout (with the notable exception of ~~1984-85~~ 1984-1985 when it was buried following sustained explosive eruptions) (Kyle et al., 1990).

23 The stable convective behaviour of the Erebus lava lake is punctuated by
24 intermittent (De Lauro et al., 2009) Strombolian eruptions associated with
25 the rupture of large (decametric) gas bubbles at the lake surface (Dibble
26 et al., 2008; Gerst et al., 2013). Phases of increased and more intense Strom-
27 bolian activity recur, lasting ~~1–10~~ 1–10 months and are followed by more
28 extended intervals during which gas bubble bursts are ~~of a much smaller~~
29 ~~(order 1m)~~ less frequent and of a smaller size (see for example Jones et al.
30 (2008)). The chemical and mineralogical composition of erupted lavas has
31 remained constant for approximately 17 ka and the abundance of unusually
32 large anorthoclase crystals is indicative of sustained shallow magma convec-
33 tion throughout this period (Kelly et al., 2008). Indeed, the presence of such
34 large crystals may be a significant influence ~~in~~ on the behaviour of the shal-
35 low convection at Erebus (Molina et al., 2012). Other properties of the lake
36 also demonstrate remarkably consistent long-term behaviour, for example
37 SO₂ flux (Sweeney et al., 2008) and radiant heat output (Wright and Pilger,
38 2008).

39 On shorter time scales, many of the lake’s properties exhibit a pronounced
40 pulsatory behaviour. Oppenheimer et al. (2009) observed that the surface
41 temperature, surface velocity and magmatic gas concentration ratios all oscil-
42 lated with a period of ~ 10 min. The cycles appeared to be phase locked with
43 each other, suggesting a common mechanism was responsible for the oscilla-
44 tions in each property. Evidence of similar cyclicality has also been observed in
45 the SO₂ flux (Boichu et al., 2010), and the H₂/SO₂ ratio (Moussallam et al.,
46 2012), but these have yet to be linked definitively to the cycles observed by
47 Oppenheimer et al. (2009).

48 One possible explanation for the observed behaviour is pulsatory exchange
49 flow of hot, degassing magma into the lake from the subjacent conduit. It has
50 been shown experimentally that given two liquids flowing in opposite direc-
51 tions in a vertical pipe (for example driven by a density difference between
52 them), ~~at sufficiently low Reynolds numbers~~ under certain flow conditions
53 an instability occurs which results in a pulsed flow (Huppert and Hallworth,
54 2007). Oppenheimer et al. (2009) suggested that such a system may exist
55 at Erebus volcano, with bubbly and degassing, low density magma rising up
56 the conduit into the lake whilst degassed, denser magma sinks back down
57 the conduit again. The resulting pulsatory flow delivers packets of fresh
58 magma into the lake quasi-periodically, giving rise to the observed cycles in
59 lake properties. The period of the cycles would be expected to reflect the
60 rheological properties of the bubbly flow and geometry of the conduit.

61 The previous studies at Erebus have analysed only very short time series
62 of data, and no investigation of the long-term behaviour of the cycles has
63 yet been conducted. However, thermal infrared (IR) images of the Erebus
64 lava lake have been collected almost every year since 2004 during the Mount
65 Erebus Volcano Observatory's annual austral summer field campaign. Using
66 a similar technique to that of Oppenheimer et al. (2009) we have extracted
67 mean surface speed estimates from the usable portions of the now substantial
68 IR dataset. Using the mean surface speed as a proxy to assess the cyclicity of
69 the lake motion, we present an overview of its behaviour between 2004 and
70 2011 and compare this to visible changes in the lake's appearance. Using a
71 dataset recorded at higher time resolution in 2010, we identify times when
72 bubbles arrive at the surface of the lake and compare this to the phase of the

73 cycles.

74 Our specific aims are to identify the persistence of the cyclic behaviour
75 within and between field seasons; to search for any variability in cycle length
76 that might point to changes in lake/conduit geometry or rheological charac-
77 teristics of the magma; and to probe further the origins of the remarkable
78 cyclic behaviour of the lava lake. We also compare observations at Erebus
79 with those for other active lava lakes.

80 **2. Summary of Activity**

81 In the following analyses, data from field campaigns between 2004 and
82 2011 have been used. Although the general behaviour of the lava lake at
83 Erebus is fairly consistent from year to year, there are some observable
84 variations. It is therefore important to set the results presented here within
85 the context of the state of activity of the lake during each of the respective
86 field campaigns.

87 Figure 1 shows how the visible surface area of the lava lake has changed
88 throughout the period of study. Possible reasons for this change are discussed
89 in detail in the following sections. Despite the reduction in visible surface area
90 from 2004 onwards, there have been no observable changes in the behaviour of
91 the lava lake. Stable convective behaviour has been maintained throughout.

92
93 A study of explosive events (due to large bubbles) between 2003–2011
94 using seismic data (Knox, 2012) shows that, with the notable exception of
95 2006–2007, the frequency of explosive events has remained fairly constant
96 at a few per week. Explosions are generally quite small, with ejecta being

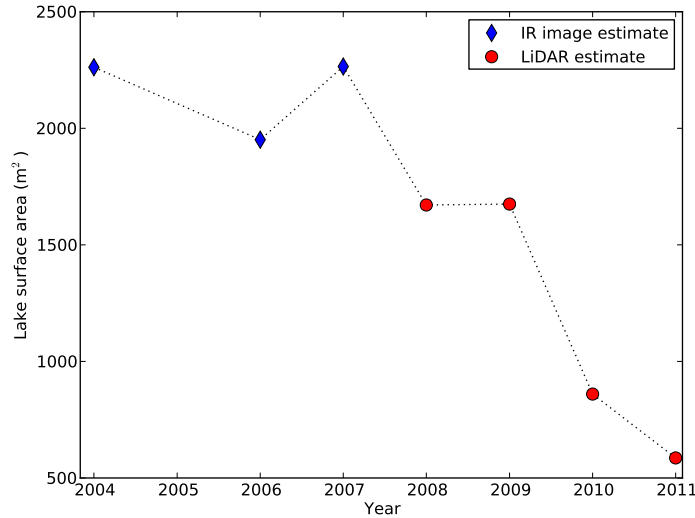


Figure 1: Surface area of the Erebus lava lake by year. The areas have been estimated from a combination of terrestrial laser scan data (provided by Jones and Frechette) and rectified IR images.

97 entirely confined to the crater. During 2006–2007 however, there were several
98 explosions per day, often of sufficient magnitude to propel ejecta out of the
99 crater.

100 We describe bubbles as “large” if they result in significant ejection of
101 material from the lake. Such bubbles are typically 10–30 m in diameter and
102 cause a visible emptying of the lake. We classify such events as being distinct
103 from the far more frequently occurring metre and sub-metre scale bubbles
104 which arrive at the surface of the lake, but do not result in explosive activity.

105

106 3. Methodology

107 Fieldwork on Erebus volcano is limited to the austral summer, and typi-
108 cally takes place from mid-November to early January. Where we refer to a
109 field season by year, we are referring to the year in which it began. The logis-
110 tics involved in reaching the crater rim, combined with frequent bad weather
111 mean that IR image data are typically only recorded for a few weeks each
112 year. The intervals of useful data are further reduced due to fluctuations in
113 the IR transmission between camera and lava lake. When the gas/aerosol
114 plume is highly condensed (high relative humidity) the IR transmission in
115 the camera waveband is poor and the images of the lake are of unusable qual-
116 ity. The latest IR camera system, which was deployed in December 2012, runs
117 continuously year-round (dependent on power) ~~(?)~~ (Peters et al., 2014). The
118 data from this fully automated system will be analysed in future work.

119 3.1. Camera Hardware

120 All IR images of the Erebus lava lake used in this study were recorded
121 by tripod-mounted camera systems installed at the Shackleton's Cairn site
122 on the northern side of the Main Crater. Three different IR camera systems
123 have been used on Erebus since 2004. The first of these was an Agema
124 Thermovision 550 mid-infrared camera, as described by Oppenheimer et al.
125 (2004), which acquired images with a 4 s time-step. The second was a FLIR
126 P25 camera equipped with a 72 mm IR lens. This camera has an uncooled
127 320×240 element detector with a spectral range of $7.5\text{--}13\text{--}13\ \mu\text{m}$ and a spatial
128 resolution (instantaneous field of view) of 0.31 mrad. The low temperatures
129 at the crater rim of Erebus severely impacted the P25's ability to write images

130 to its compact flash card, and as a result the interval between successive
131 images varies between 8 and 20 s. The most recent IR camera is a FLIR
132 SC645, with an uncooled 640×480 element detector, spectral range of 7.5-
133 ~~13~~13 μm , and a spatial resolution of 0.69 mrad. Although the SC645 is
134 capable of frame rates of up to 25 Hz, we have typically acquired images at 2 s
135 intervals. It was, however, operated with a 0.5 s time-step in acquisitions for
136 a part of the 2010 field season and we have used these higher time resolution
137 data for the bubble event analysis section of this study.

138 *3.2. Data Selection*

139 Interruptions to the recording of IR images on Erebus are common. The
140 Agema and P25 cameras both required their memory cards to be changed
141 regularly and equipment failure was frequent due to the harsh operating con-
142 ditions. These factors have resulted in a segmented data set, with many gaps.
143 The first step in data selection was to split the data into groups of continu-
144 ous acquisition that contained no two images more than 40 s apart. Groups
145 spanning less than one hour of acquisition were discarded. Subsequent data
146 processing was performed on a per group basis.

147 High winds at the summit of Erebus cause camera shake, potentially
148 introducing large errors into the velocity estimates calculated by the mo-
149 tion tracking algorithm. This problem is particularly acute in data from
150 the Agema and P25 cameras, which did not have such stable tripod mounts
151 as does the new SC645 system. Attempted stabilisation of the images in
152 post-processing failed due to the lack of distinctive stationary features in
153 the images. Instead, a simpler approach was followed, in which only peri-
154 ods of data with little or no camera shake were analysed. Due to the large

155 volume of available data, an automated routine for identifying such periods
156 was developed. This involved first defining the bounding box of the lake in
157 each image by thresholding the image at a predetermined level, and identi-
158 fying the non-zero region. Images in which the bounding box could not be
159 found, or was unusually small were rejected, as these characteristics point to
160 poor visibility of the lake (typically caused by high relative humidity, blow-
161 ing snow, or hoar-frost accumulation on the lens). The centre coordinates of
162 the bounding boxes were then assigned to clusters using SciPy’s *fclusterdata*
163 function (Jones et al., 2001). To reduce the run time of the clustering algo-
164 rithm, duplicate bounding box positions were discarded before clusters were
165 computed. Using the standard deviation of the bounding box coordinates
166 in each cluster as an indicator of camera shake, the best clusters for each
167 year (typically with a standard deviation of < 1.0 pixels) were selected. As
168 a final check of data quality, the images in each cluster were compiled into a
169 video which was then viewed to ensure good visibility of the lake and minimal
170 camera shake throughout.

171 3.3. Motion Tracking

172 Since the focal plane of the thermal camera is not parallel to the sur-
173 face of the lava lake, perspective effects mean that each pixel in the image
174 represents a different distance in the plane of the lake. To correct for this
175 distortion, each image is rectified before the motion tracking is carried out.
176 The required transformation is calculated by matching points in the image
177 to points in a terrestrial laser scan (~~TLS~~) of the lake. OpenCV’s (Brad-
178 ski, 2000) *cvFindHomography* function is then used to calculate the required
179 transformation matrix, and the *cvWarpPerspective* function used to apply it

180 (see Bradski and Kaehler (2008)). ~~FLS~~Correcting the images in this way
181 also accounts for any lens distortion. Terrestrial laser scan data of the lava
182 lake were only available for 2008 onwards. For thermal images from earlier
183 years, the homography matrix is calculated from the viewing angle of the
184 camera and the size of the lake (which had been estimated with a handheld
185 laser range finder). Although this method neglects lens distortion, we expect
186 the effects to have little impact on the results obtained.

187 The significant temperature contrast between the lake and the surround-
188 ing crater causes problems for the feature tracking algorithm. As the strongest
189 feature in the image, the lake boundary tends to dominate over the structure
190 within the lake that we are actually interested in. This issue can be overcome
191 by masking the regions outside of the lake with Gaussian-distributed white
192 noise with a mean and variance similar to that of the pixels within the lake.
193 Random noise is used rather than a fixed value to prevent the output of the
194 bandpass filters used in the wavelet decomposition from being exactly zero,
195 as this causes the algorithm to fail.

196 The feature tracking algorithm itself is based on the Dual-Tree Complex
197 Wavelet Transform (DT-CWT) (Kingsbury, 2001). Unlike the widely used
198 Discrete Wavelet Transform (DWT) (see for example Polikar (2010)), DT-
199 CWT is approximately shift invariant, meaning that shifts in input signal
200 do not cause changes in energy distribution between wavelet coefficients at
201 different scales. Instead, it is found that shifts in the input signal manifest
202 themselves as a phase shift between the wavelet coefficients. By decomposing
203 each frame in a series of images using the DT-CWT and comparing the phase
204 shifts between the subimages, it is possible to estimate the displacement field

205 that maps features in one frame to the next. The estimate is first made at a
206 coarse level of decomposition, with subsequent estimates made at finer levels
207 so as to refine the result (Magarey and Kingsbury, 1998). Oppenheimer
208 et al. (2009) tuned the method specifically for working with IR images from
209 Erebus volcano, and we adopt the same parameters for the motion estimation
210 reported here. The algorithm was verified by passing in sets of two identical
211 images, one of which was shifted by a known amount and checking that the
212 shift was correctly detected. Further verification was achieved by comparing
213 velocity estimates obtained from the algorithm with visual estimates found
214 by counting pixels.

215 Finally, the mean surface speed of the lake was found by averaging the
216 magnitudes of the computed velocity vectors. To avoid possible edge effects,
217 only velocity vectors from the central region (at least 3 pixels inside the lake
218 boundary) of the lake were included in the averaging.

219 *3.4. Time Series Analysis*

220 As can be seen in Fig. 2, the mean surface speed time series obtained are
221 highly non-stationary. To evaluate the periodic components of the series with
222 time, we therefore use a Morlet wavelet transform to produce spectrograms
223 of the data. Our implementation of the Morlet transform is the same as that
224 of Boichu et al. (2010). The mean speed data were interpolated to a uniform
225 1 s time step prior to the Morlet transform using simple linear interpolation.

226
227 As illustrated by the expanded regions in Fig. 2, ~~the higher frequency~~
228 ~~components of the signal tend to be of lower amplitude, and are easily missed~~
229 ~~in spectrograms~~ some of the ~ 10 min cycles are of much greater amplitude

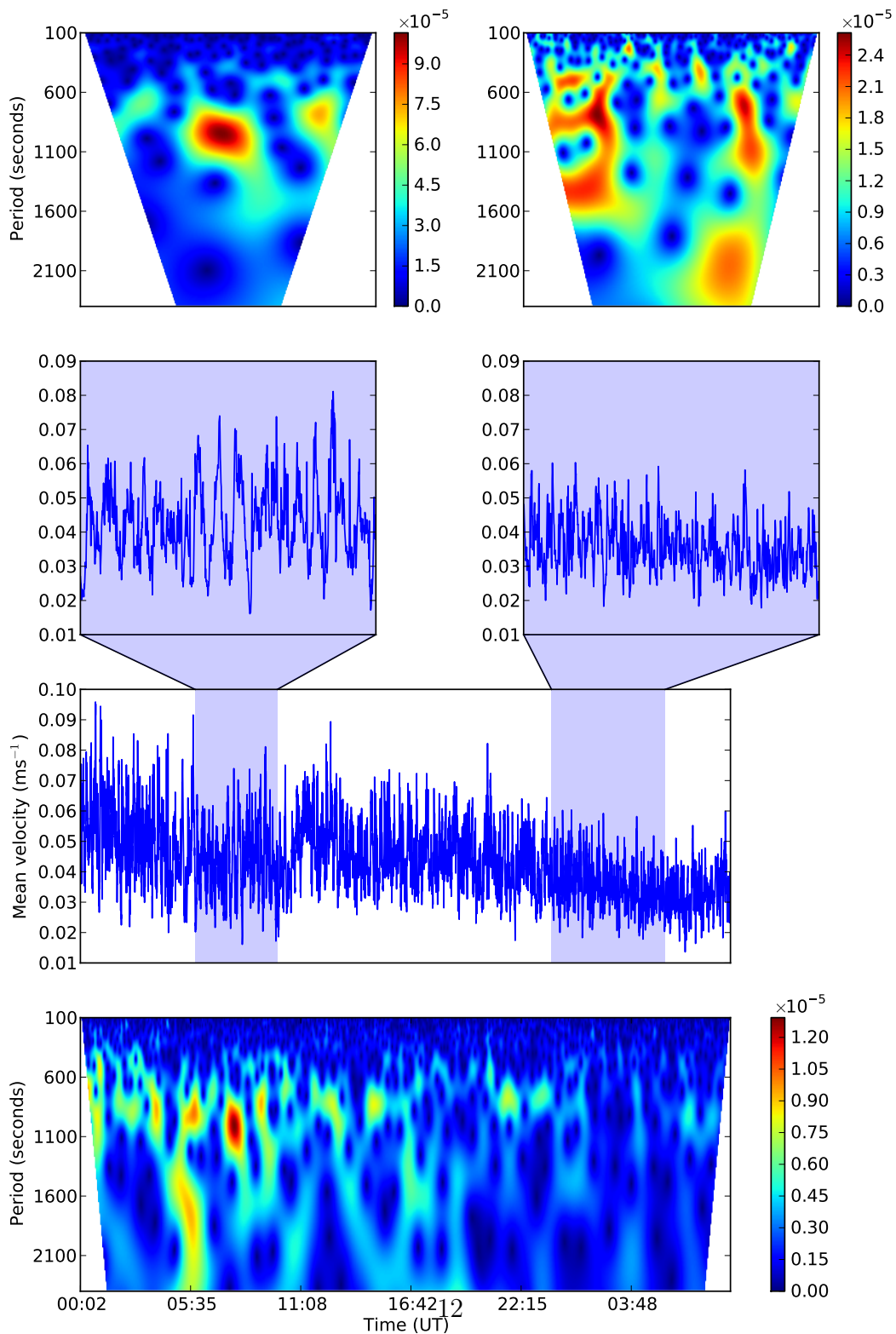


Figure 2: Selection of mean surface velocity data from December 2010 and the corresponding Morlet ~~periodogram~~-wavelet transform (modulus) showing the periodicities present. The expanded sections show how an increase in period is accompanied by an increase in amplitude.

230 than others, and will result in a very high modulus in the Morlet transform.
231 Longer time series tend to exacerbate this problem, since they often contain
232 at least a few very high amplitude oscillations, which then saturate the colour
233 scale and mask much of the other detail. In this way, the cyclicity of the lake
234 may not be apparent even if it exists. However, creating a spectrogram of just
235 the data from the “non-cyclic” time period, reveals that there are indeed still
236 ~~periodic components~~ ~10 min period components present, they are simply of
237 lower amplitude. This is also apparent in the mean speed time series data.

238 3.5. Bubbles

239 Bubbles breaking the surface of the lake manifest themselves as sharp
240 peaks in the mean surface speed time series. The poor time resolution of
241 the Agema and P25 cameras mean that most bubbles are not recorded.
242 However, much of the SC645 data from 2010 was recorded at 2 Hz, which
243 is more than sufficient to capture when bubbles arrive at the surface. ~~A~~
244 ~~manual comparison of the spikes in speed with bubble size (as viewed in the~~
245 ~~images themselves) revealed that there was no obvious correlation between~~
246 ~~the surface speed peak height and the bubble size. The following analysis~~
247 ~~therefore makes no distinction between small and large bubbles. However,~~
248 ~~since larger bubble bursts (i.e. those that eject lava out of the lake) are~~
249 ~~relatively rare at Erebus, the majority of events are small (metre-scale)~~
250 ~~bubble bursts.~~

251 Bubble events were located by comparing the mean speed time series to
252 a low-pass filtered copy of itself. Bubbles were classified as events where the
253 speed was greater than 1.2 standard deviations above the filtered value. The
254 value of 1.2 was chosen by comparing bubble events detected by the algorithm

255 to those located manually in a test set of data spanning three hours. The
256 analysis was conducted on a continuous time series of good quality data from
257 24 December 2010, spanning approximately 13 h. By visually inspecting the
258 IR images corresponding to each of the bubble events, we determined that all
259 events were small (metre-scale, with no ejection of material from the lake).

260 The bubble events detected are uniformly distributed in time. However,
261 this tells us nothing of how they are related to the pulsatory behaviour of
262 the lake. What is of real interest is how bubble events relate to the phase
263 of the speed cycles, for example, do more bubbles surface during periods of
264 fast surface movement? In order to evaluate a possible relationship between
265 the cyclicity and bubble events we use the method of delays (e.g. Kantz
266 and Schreiber (2003)) to reconstruct our time series data into a phase space
267 representation. If the bubble events are somehow correlated to the phase of
268 the speed cycles then we argue that their distribution in phase space will differ
269 from that of a random sample taken from the time series. We can imagine
270 this as being due to a clustering of bubble events at certain positions in phase
271 space. Details of the phase space reconstruction are given in Appendix A
272 where we show that in order to accurately represent our time series, a 4-
273 dimensional phase space (embedding dimension of 4) is required. The data
274 were low-pass filtered prior to phase space reconstruction to remove noise
275 and the spikes due to bubbles.

276 The time series analysed contains 141 bubble events (Fig. 3). We com-
277 pared the cumulative distribution function (CDF) of the bubble events to a
278 reference CDF in each of the phase space dimensions. The reference CDF
279 is the CDF of the time series data itself. As an indicator of the expected

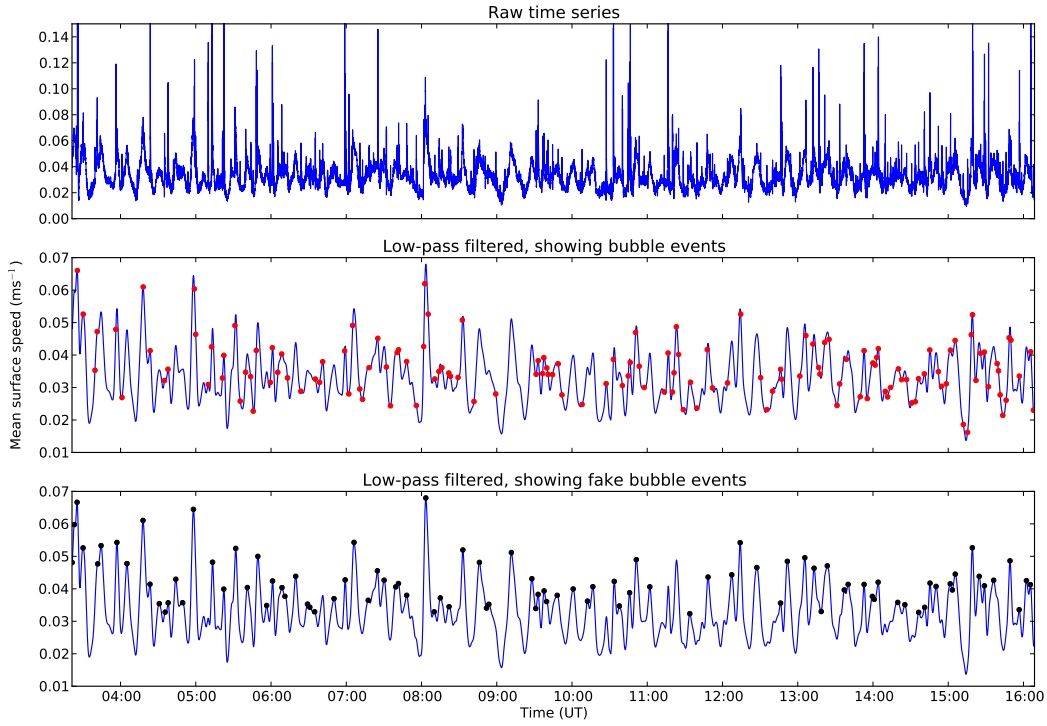


Figure 3: Top panel: time series of mean lake surface speeds from 24 December 2010. Middle panel: the same data, low-pass filtered to remove noise and spikes due to bubbles and with bubble events marked. Bottom panel: low-pass filtered data with the fake bubble events used for testing marked.

280 variation in CDFs, the standard deviation of 10,000 CDFs, each constructed
 281 from 141 points randomly sampled from the time series was computed. A
 282 significant variation of the bubble event CDF from that of the reference
 283 in any of the dimensions, would indicate some correlation to the phase of
 284 the cycle. Differences between CDFs were quantified using the two-sample
 285 Kolmogorov-Smirnov test (K-S test). The computed critical value for the
 286 K-S test at 90% confidence (based on a reference sample size of 90901, and
 287 a bubble event sample size of 141) is 0.102.

288 To verify the technique, we created a set of 95 fake bubble events located
289 at the peaks of the mean speed cycles (Fig. 3). These events were then sub-
290 jected to the same analysis as the real bubble events. The critical value for
291 the K-S test at 90% confidence is 0.125 for the fake bubble sample size of 95.
292 As shown in Fig. 4, the CDFs for the fake bubble events show a strong devia-
293 tion from that of the random samples in each of the phase space dimensions,
294 with K-S test results of 0.50, 0.15, 0.16 and 0.13 respectively (i.e. all above
295 the critical K-S value, suggesting the two samples came from different distri-
296 butions). Hence, the technique correctly identified the correlation between
297 the fake bubble events and the phase of the speed cycles.

298 **4. Results**

299 The 2010 field season was characterised by exceptional visibility of the
300 lava lake. In addition to the IR images captured, several short time series
301 of visible images were captured using a digital SLR camera equipped with
302 a telephoto lens. Figure 5 shows a short time series of mean surface speed
303 and mean surface temperature data calculated from IR images, with visible
304 images corresponding to peaks and troughs in the speed also shown. There
305 are no consistent differences observed between the appearance of the lake
306 surface during periods of high speeds and periods of low speeds.

307 Oppenheimer et al. (2009) found a strong correlation between the phase
308 of cycles in mean surface speed and mean surface temperature in their data
309 set. This correlation is further demonstrated by the time series shown in
310 Fig. 5 and Fig. 6. Note however, that since we have not attempted an ac-
311 curate temperature calibration of the IR images, we present mean surface

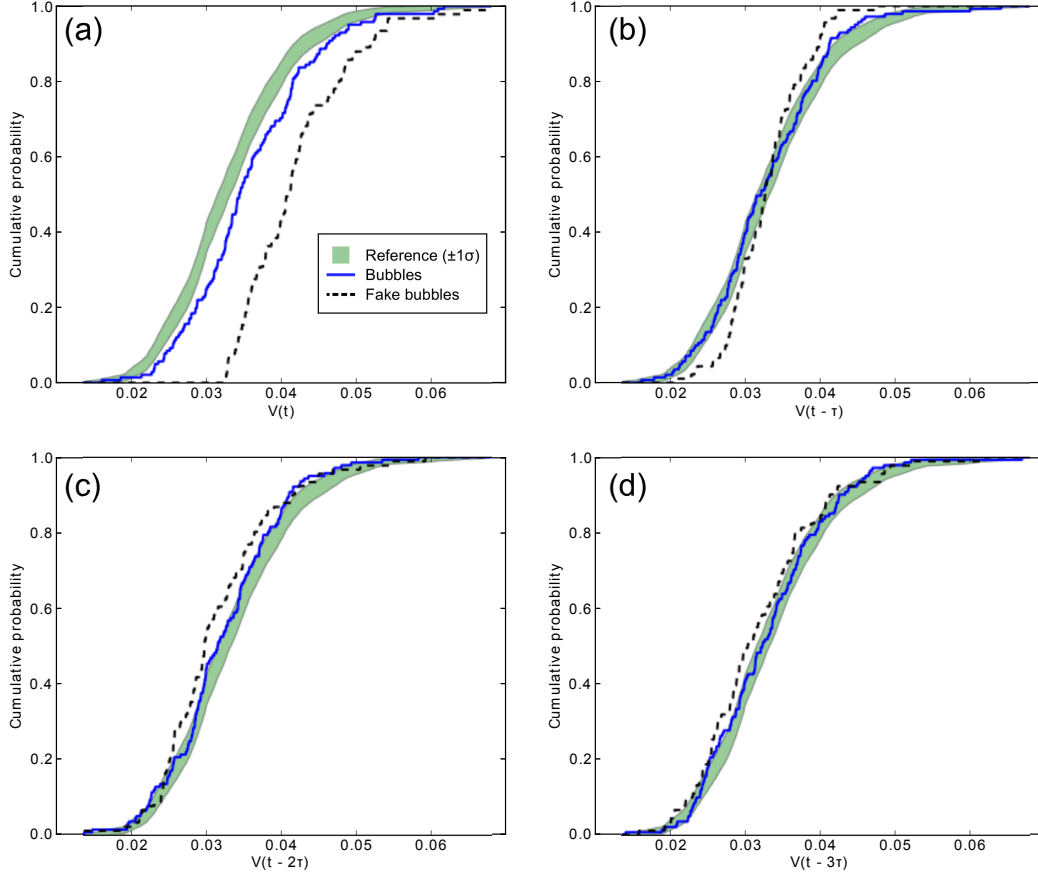


Figure 4: The cumulative distribution functions (CDFs) in each of the four phase space dimensions for the bubble events (solid line) and fake bubble events (dashed line). The x-axes represent the coordinates of the events in the corresponding phase space dimension, from the zero-lags dimension, $V(t)$, up to the three-lags dimension, $V(t - 3\tau)$, where $\tau=150$ s (see Appendix A). The shaded region represents one standard deviation on either side of the reference CDF (i.e. the CDF of the mean speed data). Large deviations from the reference CDF are indicative of a correlation with the phase of the speed cycles, as can be seen in the fake bubble data. The deviation from the reference in the first dimension (a) of the bubbles CDF is attributed to imperfect filtering of the signal rather than a phase dependence.

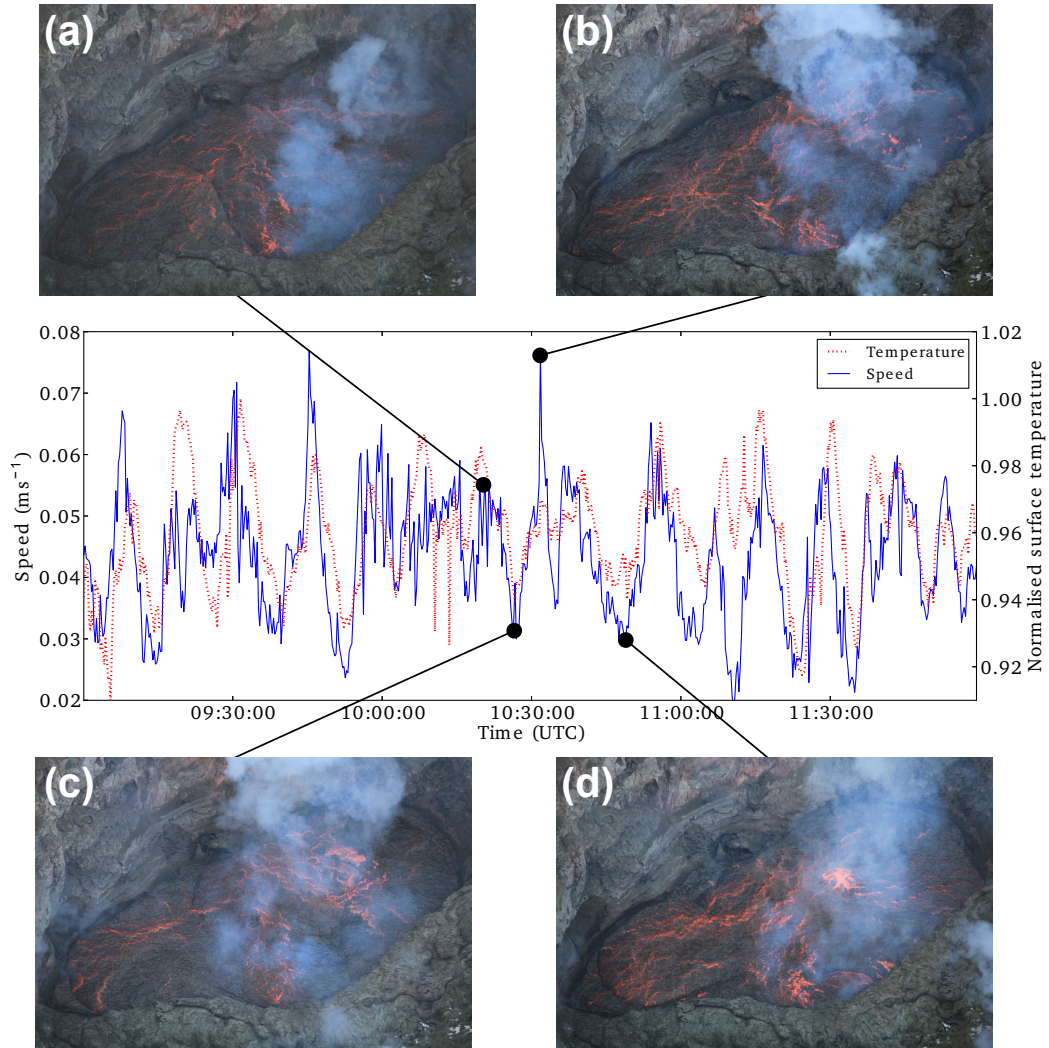


Figure 5: Time series of mean lake surface speed from 17 December 2010, with photographs showing the appearance of the lake surface at periods of high surface speed (a,b) and low surface speed (c,d). There is no distinct difference between the appearance of the lake surface during periods of high or low surface motion. Note that in (d), a small gas bubble can be seen just reaching the surface. The lake is approximately 40 m across its long axis.

312 temperatures normalised to their maximum value. These values are linearly
313 proportional to the real temperature. What is not clear from these data
314 alone, is whether the temperature variations observed are due to a genuine
315 increase in the temperature of the lava in the lake, or due to an increase in the
316 number of cracks in the surface crust of the lake caused by the increased mo-
317 tion. Additional cracks will expose more of the underlying lava to the surface
318 and will therefore cause an increase in the mean temperature recorded by the
319 IR camera. Increased cracking during periods of higher surface speed is not
320 ~~evident obvious~~ in the images shown in Fig. 5, ~~indicating that the change in~~
321 ~~recorded temperatures~~ suggesting that the changes in recorded temperature
322 are indeed due to an increase in lake temperature. However, we feel that a
323 qualitative argument such as this is insufficient to rule out increased cracking
324 as a cause.

325 In an attempt to more rigorously identify the reason for the temperature
326 cycles, we compared the histograms of the thermal images at the minima
327 and maxima of the cycles. If the cycles are caused by an increase in lake
328 temperature, then we would expect the histograms at the cycle maxima to
329 be shifted relative to those at the minima. If increased cracking is the cause,
330 we would expect more high temperature pixels, resulting in a skewing of the
331 histograms at the maxima compared to those at the minima. Unfortunately,
332 the results obtained were ambiguous, with greater differences between histograms
333 from the same point in the cycles than comparing those at maxima to those
334 at minima. The cause of the measured temperature fluctuations remains
335 elusive, however, it seems likely that they are caused by a combination of
336 both increased surface cracking and increased lake temperature.

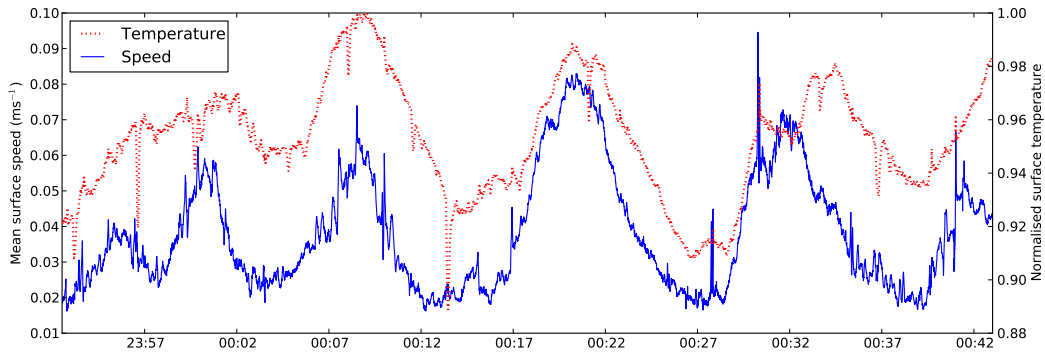


Figure 6: Short time series of mean surface velocity and mean surface temperature data from ~~21-22~~21-22 December 2010 calculated from images acquired with the SC645 camera. We have not attempted to retrieve accurate temperatures from the images, and instead report unitless temperature values normalised by the maximum value in the time series. The pulsatory behaviour is particularly clear during this period, and the symmetry of the peaks about their centre is evident.

337 Figure 6 shows a short time series of mean surface speed and mean sur-
 338 face temperature calculated from IR images captured in 2010. The pulsatory
 339 behaviour was particularly pronounced during the period shown, and the
 340 waveform of the cycles is clear. The peaks in speed/temperature are approx-
 341 imately Gaussian in shape, with rising and falling edges that are symmetric
 342 about the centre of the peak. The peaks tend to be shorter lived than the
 343 troughs, suggesting a system with a stable baseline state that is being per-
 344 turbed, rather than a system that is oscillating about a mid-point.

345 Morlet spectrograms of the mean speed data from ~~2007-2011~~the 2007-2011
 346 field seasons are provided as supplementary material to the online version of
 347 this article. What is clear from the data is that the cycles in speed are not
 348 strictly periodic. Instead, there tends to be a broad range of periodic compo-
 349 nents present, centred at around 900 s. However, these components appear

350 to be fairly consistent across the dataset and have not changed appreciably
351 during the period of study. Figure 7 further illustrates this point, showing the
352 time average ~~of~~ (normalised to have a mean of zero and standard deviation
353 of one) of the modulus of all the Morlet spectrograms from each field season.
354 The general trend towards higher modulus at longer periods is due to the fact
355 that long period variations in mean speed tend to be of greater amplitude
356 than short period variations (as is typical for most time series data from
357 natural systems). Despite this, the broad peak around 900 s is evident in
358 the data from ~~2007-2011~~ the 2007–2011 field seasons. The time series from
359 the 2004 and 2006 field seasons were of insufficient duration to allow analysis
360 for long period behaviour, and as a result do not show the same behaviour
361 as the other years. ~~As~~ It is unfortunate that the dataset from 2006, when
362 Erebus underwent a period of increased explosive activity, is of insufficient
363 length to compare to other years. However, as shown in Fig. 8, the pulsatory
364 behaviour of the lake ~~also~~ appears to be robust against ~~large perturbations~~
365 perturbations caused by large bubbles. The figure shows a short time se-
366 ries of mean surface velocity data from ~~29-30~~ 29-30 December 2010, during
367 which a large (~ 30 m) bubble arrives at the surface of the lake. Despite
368 a significant ejection of material from the lake, ~~the Morlet spectrogram of~~
369 ~~the~~ speed data shows that the pulsatory behaviour appears to be uninter-
370 rupted. It is interesting to note that at the time of the explosion the Morlet
371 spectrogram shows a particularly strong periodic component at ~ 1000 s. We
372 believe that this may be caused by increased surface speeds in the build-up
373 to the explosion and also during the recovery phase as the lake refills. The
374 IR images show that the lake level rises rapidly immediately prior to a large

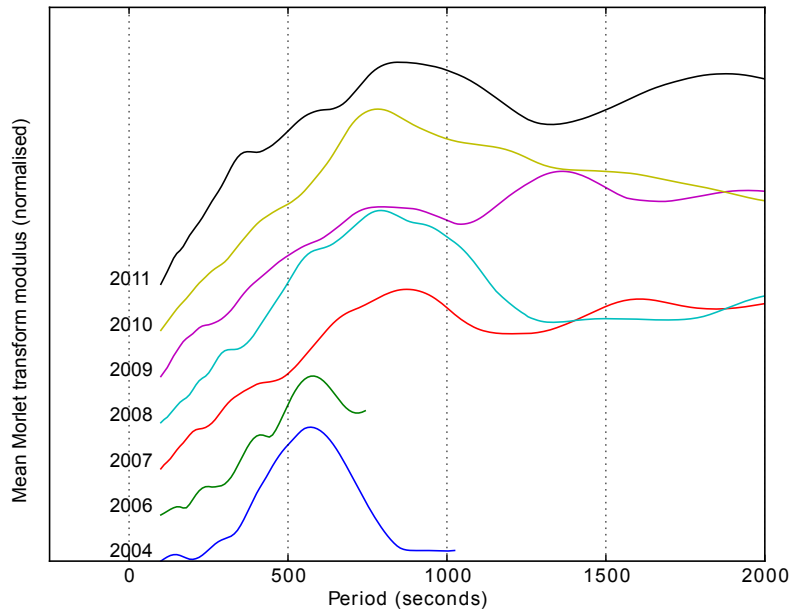


Figure 7: Time-Normalised time averages of the Morlet periodograms-transform modulus of all available data from each field season. The data from each year have been vertically offset from each other for clarity. A broad peak corresponding to the period of the lake cycles (~900 s) is evident in the 2007–2011 data. The time series from the 2004 and 2006 field seasons were of insufficient length to be able to resolve long period fluctuations.

375 bubble reaching the surface, likely causing an increase in the recorded surface
 376 speed. Rapid flow of lava into the lake during the refill phase of an explosive
 377 event is also likely to cause elevated surface speeds.

378 In addition to the apparent stability of cycles in surface speed, the magni-
 379 tude of the surface speed has also remained approximately unchanged since
 380 2004. Although the mean surface speed can exhibit considerable variabil-
 381 ity ($\sim 3-20$ cm s^{-1}) on a timescale of days, no systematic change was
 382 observed over the period of study.

383 Whilst the behaviour of the mean surface speed has remained remarkably

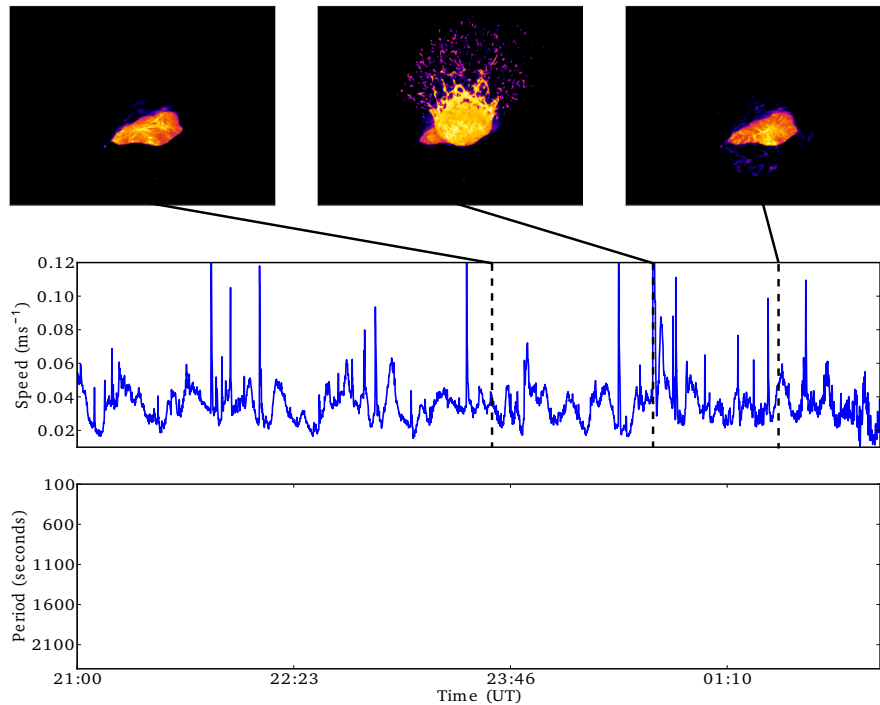


Figure 8: A 35 h time series of mean surface ~~velocity~~ speed data from the ~~29-30-29-30~~ 29-30 December 2010 calculated from images acquired with the SC645 camera and the corresponding Morlet spectrogram. The IR images above show the state of the lake before, during and after a large (~ 30 m) bubble burst. ~~The Cycles of between $\sim 600 - 1100$ s are visible across the time series both in the Morlet spectrogram shows that and in the eyelie behaviour of mean speed data. The strong ~ 1000 s signal in the lake appears spectrogram corresponding to the explosion itself may be unaffected caused by elevated speeds due to the arrival rising of the bubble lake level prior to the explosion and the ~ 900 s period band persists across subsequent refilling of the full time series lake afterwards.~~

384 stable, the visual appearance of the lava lake has changed significantly. Fig-
385 ure 1 shows how the surface area of the lake (calculated from IR images and
386 ~~TLS~~terrestrial laser scan data) has decreased since the first measurements
387 in 2004. Overall the surface area has reduced by a factor of approximately
388 four. The ~~TLS~~terrestrial laser scan data also show that since at least 2008
389 (when the first ~~TLS~~terrestrial laser scan data were recorded), the decrease
390 in area has been accompanied by a ~~3-4~~3-4m per year drop in lake surface
391 elevation (Jones and Frechette, pers. comm., 2012). The dramatic reduc-
392 tion in surface area cannot be accounted for by the drop in surface elevation
393 (i.e. due to the lake receding into a conical basin) since the lake walls are
394 observed (~~TLS~~terrestrial laser scan data and visual observations) to have
395 a near-vertical profile. That the cyclic behaviour in surface speed of the
396 lake is unaffected by lake geometry would be strong evidence to suggest that
397 the cycles are driven by processes occurring deeper in the magmatic system
398 rather than in the lake itself. It is difficult to ascertain, however, whether
399 the observed reduction in surface area is due to a change in lake geometry, or
400 instead, due to the formation of a cooled crust over part of the lake, with ac-
401 tive lake persisting beneath. The sequence of images shown in Fig. 9 provides
402 evidence for the latter case. A puff of gas is seen to emerge from a vent some
403 tens of metres away from the visible edge of the lake. A few seconds later,
404 a puff of gas is seen to emerge from a source at the edge of the lake closest
405 to the vent. Such behaviour could be caused by a bubble (or by a more dis-
406 tributed bubbly flow) reaching the lake surface beneath a cooled crust. The
407 gas would be forced to travel laterally until it could escape through the vent,
408 and some time later at the edge of the crust. However, the “cooled crust”

Surface area of the Erebus lava lake by year. The areas have been estimated from a combination of TLS data (provided by Jones and Frechette) and rectified IR images.

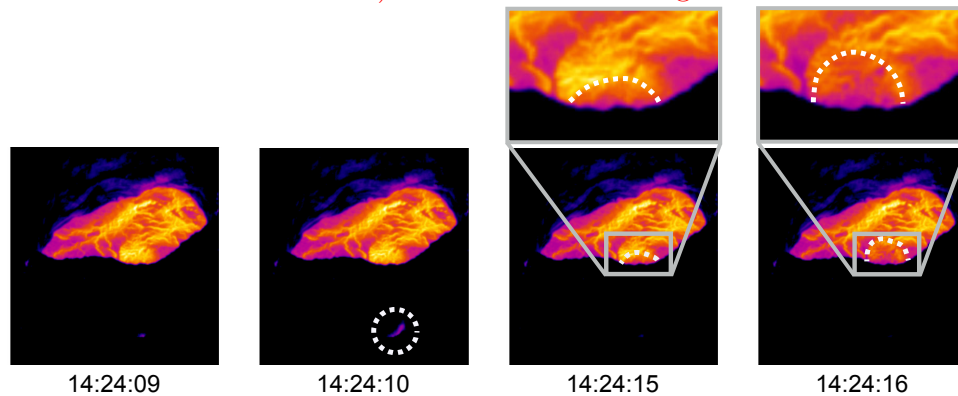


Figure 9: A series of IR images from 19 December 2010 recorded using the SC645 camera. A puff of gas is seen to emerge from the vent in the foreground at 14:24:10–10 (highlighted with dashed circle). A few seconds later a puff of gas emerges from the side of the lake closest to the vent (highlighted with dashed line). This observation suggests that only part of the lava lake surface is visible. The lake extends beneath a “lid” of a former lake high-stand and ejecta.

409 hypothesis is somewhat contradicted by observations of the refilling of the
 410 lake following large bubble bursts. The lake is seen to refill from below over
 411 a period of several minutes, with no evidence of lava flowing outwards from
 412 beneath the potentially crusted region. Further study is required to fully
 413 determine the reasons for the change in visible lake area and it is hoped that
 414 this may be possible with the longer time series of thermal images which are
 415 now becoming available.

416 Figure 4 shows the CDFs cumulative distribution functions (CDFs) of the
 417 bubble events, and fake bubble events in each of the four phase space dimen-

418 sions. The shaded areas delimit one standard deviation on either side of the
419 reference CDFs. As already discussed, the CDFs for the fake bubbles show
420 a strong deviation from the reference, correctly identifying the correlation
421 between the phase of the speed data and the fake bubble events. In contrast,
422 the CDFs for the real bubble events are very similar to the reference in all but
423 the first dimension. The K-S test gives values of 0.15, 0.05, 0.07 and 0.06 for
424 the four dimensions, respectively. Apart from the first dimension, these are
425 all below the critical K-S value at 90% confidence (0.102), indicating that the
426 bubble events are from the same distribution as the speed data itself and that
427 there is therefore no correlation between the phase of the speed cycles and
428 the bubbles. In the first dimension, the CDF of the bubble events appears
429 to be the same shape as that of the mean speed data, but shifted slightly to
430 the right (higher mean speed). We believe that this is caused by the failure
431 of our low-pass filtering to remove fully the spikes caused by bubble events
432 in the mean speed data, rather than any correlation with the phase of the
433 cycles. As a result, bubble events appear to occur at slightly higher speeds
434 than they actually do, shifting the CDF to the right. We tested this hypoth-
435 esis by plotting the CDF of 141 randomly selected points from the speed
436 data with a linear offset of 0.002 ms^{-1} added. The results showed a CDF
437 that matched that of the mean speed data in all dimensions except the first,
438 which showed a linear offset to the right as expected. We therefore conclude
439 that the bubble events are not correlated to the phase of the velocity cycles
440 and that the deviation we observe in the first dimension is due to the low-
441 pass filter's inability to totally remove the effects of bubble events from the
442 underlying mean speed signal.

443 5. Discussion

444 A common conclusion of multi-year studies conducted at Erebus volcano
445 is that its behaviour is remarkably stable. Observations of radiant heat out-
446 put (Wright and Pilger, 2008), SO₂ flux (Sweeney et al., 2008) and seismicity
447 (Aster et al., 2003) have all found very little variation during the past decade.
448 Our findings that the pulsatory behaviour of the lava lake has been a persis-
449 tent and unchanging feature (both on a daily and a yearly time-scale) since
450 at least 2004 fit well with these previous findings and further emphasise the
451 remarkable stability of Erebus’s magmatic system. The preservation of cy-
452 cles in surface speed despite large perturbations to the system (decametric
453 bubble bursts) is indicative not only of the stability of the responsible mech-
454 anism, but also that it is likely sourced at a deeper level than the lake itself.
455 This argument is further supported by the consistency of the motion cycles
456 despite the dramatic reduction in lake size. However, as already discussed,
457 it is not clear if the apparent change in lake size represents a true change in
458 geometry or simply the formation of a cooled crust over a part of the lake.

459 The broad width of the peak in the spectrograms that we observe is con-
460 sistent with the findings of Oppenheimer et al. (2009) who found the period
461 of the fluctuations in mean lake speed to vary between $\sim 4-15$ 4-15 min for the
462 2004 dataset. Although short sections of our data appear to contain several
463 discrete frequency bands within this range, such fine scale structure is never
464 observed consistently over time periods of more than a few hours. No clear
465 pattern to the variation of the period of fluctuations measured is evident from
466 the spectrograms. However, it is important to consider how well the mean
467 speed of the lake surface represents the underlying process responsible for

468 the pulsatory behaviour. Even if this process contains well defined, discrete
469 periods, complex flow dynamics and other forcing mechanisms (such as ther-
470 mal convection within the lake) may result in a highly non-linear response in
471 the surface speed. It is possible that the broad distribution in period of the
472 cycles in speed observed is due to the complex coupling between a periodic
473 driving mechanism and the flow dynamics of the lake. Given the correlation
474 between surface motion and gas composition ratios (which must have dif-
475 ferent couplings to the driving mechanism) reported by Oppenheimer et al.
476 (2009), we believe that the variability in period stems primarily from the
477 variability in the underlying driving mechanism.

478 Current theories on driving mechanisms for lava lake fluctuations can
479 be grouped into three main categories; density driven, bi-directional flow
480 of magma in the conduit feeding the lake (Oppenheimer et al., 2009), “gas
481 pistoning” caused by gas accumulation either beneath a solidified crust on
482 the surface of the lake (Patrick et al., 2011) or as a foam layer at the top of
483 the lava column (Orr and Rea, 2012), and gas bubble driven pressurisation
484 changes (Witham et al., 2006). In the latter mechanism, the (uni-directional)
485 upflow of bubbly magma in the conduit is interrupted by excess hydrostatic
486 pressure in the lake. Stagnation of the flow allows bubbles in the conduit
487 to coalesce into large gas slugs which rise to the surface independently of
488 the melt. The release of large gas slugs at the surface of the lake cause an
489 increase in pressure at the base of the conduit. If this exceeds the pressure in
490 the magma chamber then downflow occurs, suppressing the ascent of bubbles
491 in the conduit. As the lake drains the downflow reduces until it can no longer
492 suppress the ascent of bubbles, and the cycle repeats. Witham et al. (2006)

493 were able to demonstrate this mechanism by bubbling air through a water
494 column with a basin attached to the top to act as the lake. They observed
495 cyclic variations in the depth of water in the basin, consisting of a logarithmic
496 increase in depth followed by a rapid, linear decrease. As shown by Orr
497 and Rea (2012), gas pistoning is also an asymmetric process, consisting of a
498 relatively slow, cumulative deviation from the baseline state of the system
499 as bubbles are trapped in the foam layer or beneath the solidified crust,
500 followed by a sudden release of the accumulated gas and rapid return to the
501 baseline state. The symmetry of the perturbations in the Erebus lava lake
502 is not consistent with either of these mechanism. It may be argued that the
503 complex geometry of the upper magmatic system of Erebus could lead to a
504 more symmetric variation than observed by Witham et al. (2006) and Orr
505 and Rea (2012). However, our finding that the arrival of small (metre scale)
506 bubbles at the surface of the lake is uncorrelated with the phase of the speed
507 cycles is only consistent with the bi-directional flow mechanism. Both bubble
508 driven mechanisms require a periodic release of bubbles prior to lake draining
509 and in the case of the Witham et al. (2006) mechanism a significant decrease
510 in the number of bubbles during lake draining. ~~Since such behaviour is not~~
511 ~~observed (either~~ Large (decametric) bubbles, typically occur at Erebus only
512 a few times per week, and cannot therefore be responsible for the ~10 min
513 cycles. Since no periodic release of small bubbles is observed either (visually
514 e.g. Fig. 5, or statistically Fig. 4), we argue that the pulsatory behaviour of
515 the lava lake at Erebus volcano is driven by magma exchange between a
516 shallow magma chamber (Zandomenighi et al., 2013) and the lake through
517 bi-directional flow in the connecting conduit.

518 It is interesting to note that on average, bubble events in the data presented
519 in Fig. 3 occur every 5.5 min. This is comparable to the cycles in surface
520 speed, which range from ~ 4 –15 min in period. However, given that some
521 cycles occur without any bubbles surfacing (e.g. 09:00–09:15 in Fig. 3) and
522 given the random distribution of bubbles with respect to the phase of the
523 cycles (Fig. 4), we believe the similarity in period to be coincidental.

524 Pulsatory behaviour deriving from bi-directional flow in a conduit has
525 been demonstrated for single-phase systems using two fluids of different
526 densities (Huppert and Hallworth, 2007) . However, any exchange of magma
527 occurring at the Erebus lava lake will clearly be multi-phase, and its dynamics
528 will be influenced not only by the presence of gas bubbles but also by the
529 large anorthoclase crystals which constitute 30–40% of the melt volume
530 (Kelly et al., 2008) . Indeed, numerical simulations of the Erebus magmatic
531 system indicate that the inclusion of crystals has a very significant effect on
532 the flow dynamics (Molina et al., 2012) . It seems likely that gas bubbles
533 play an even more significant role than the crystals, however, a complete
534 multi-phase flow model of the Erebus system is not yet available. Whilst it is
535 possible that the dynamics observed by Huppert and Hallworth (2007) may
536 not be applicable to a complex multi-phase system such as that at Erebus,
537 the lack of compelling evidence for an alternative mechanism leads us to
538 conclude that density driven bi-directional flow is the most likely explanation
539 for the observed cyclic behaviour. As noted by Oppenheimer et al. (2009) ,
540 the density contrast driving the flow is likely to be caused primarily by
541 degassing of the magma during its occupancy of the lake, rather than by
542 heat loss.

543 It is is observed by Bouche et al. (2010) that bubbles in the lava lake at
544 Erta 'Ale volcano may be trapped beneath the cooled crust at the surface of
545 the lake and be forced to travel laterally until they encounter a crack in the
546 crust before they can surface. If such a process were also occurring in the
547 Erebus lake, then it would invalidate our comparison of the bubble events
548 to the cycles in surface speed. The variable duration of lateral migration of
549 bubbles would prevent any direct comparison of the timings of the bubble
550 events and the phase of the cycles, since it would tend to randomise their
551 arrival at the surface. However, unlike the Erta 'Ale lava lake, which has a
552 crust composed of large solid plates, the crust on the Erebus lake is thinner
553 and more fluid. It can be observed in the IR images that even small bubbles
554 ($\ll 1$ m in diameter) break the surface in areas of the lake with no visible
555 cracks. We do not therefore believe that the crust on the Erebus lake inhibits
556 bubble ascent, nor that it causes significant lateral displacement of bubbles.

557

558 In our analysis ~~, we made no distinction between small bubbles, which of~~
559 the correlation of bubble events to lake cycles, we have only looked at small
560 bubbles in detail, since the dataset did not contain any large events. Small
561 bubbles may be sourced within the lake itself, ~~and whereas~~ large (decamet-
562 ric, causing ejection of material out of the lake) bubbles ~~that~~ are thought
563 to have originated at greater depths (Oppenheimer et al., 2011; Burgisser
564 et al., 2012). It is possible that the passage of large bubbles through the
565 conduit may perturb the bi-directional flow of magma, causing ~~the observed~~
566 ~~variability~~ variations in the period of lake surface speed fluctuations. Al-
567 though no such variation was observed in Fig. 8, we do not believe this to be

568 sufficient evidence to discount such a possibility. Since the arrival of large
569 bubbles is relatively infrequent, a time series spanning several months would
570 need to be analysed to achieve a statistically significant sample size with
571 which to investigate possible effects of large bubbles on the lake’s motion.
572 We are presently working on an autonomous camera installation on Erebus
573 that we hope can provide such data ~~(?)~~(Peters et al., 2014).

574 **6. Conclusions**

575 We have reported an analysis of thermal infrared image data of the active
576 lava lake at Erebus volcano spanning seven field campaigns from ~~2004–2011~~.
577 2004–2011. In total 370,000 useful images were acquired representing 42
578 “field days” of observations and spanning contiguous observations of up to
579 44 h duration. The images were analysed using a feature-tracking algorithm
580 to determine the mean speed of the surface of the lake and this was used
581 to monitor its pulsatory behaviour. Shot noise in the mean speed data was
582 found to indicate bubbles arriving at the surface of the lake, allowing an
583 analysis of how bubbles related to the phase of the surface speed cycles.

584 Since 2004, the apparent size (surface area) of the Erebus lava lake has
585 decreased by a factor of four. However, the available evidence suggests that
586 this may not represent a true reduction in lake size, rather it is due to the
587 formation of a cooled crust over part of the surface with active lake persisting
588 beneath.

589 Despite these changes in the lake’s appearance, its pulsatory behaviour
590 has remained constant over the period of study, exhibiting cycles in mean
591 surface speed with periods in the range ~~~4–15~~~4–15 min. No obvious long-

592 term progression of the cycles was observed. Surface speed time series are not
593 symmetrical about their mean (the troughs in speed are much broader than
594 the peaks), suggesting that the pulsatory behaviour is due to intermittent
595 perturbations of the system, rather than an oscillatory mechanism.

596 Bubbles arriving at the surface of the lake show no correlation to the
597 phase of the surface speed cycles. We therefore conclude that the pulsatory
598 behaviour of the lake is driven primarily by magma exchange with a shallow
599 magma reservoir rather than by a flux of bubbles.

600 While we have analysed a substantially larger dataset than Oppenheimer
601 et al. (2009), we have still been limited by the intermittent coverage. We
602 hope that our recently-installed autonomous thermal camera system will
603 yield much more extended time series, facilitating investigations into the
604 effect of large (decametric) bubbles on the pulsatory behaviour of the lake.

605 **7. Acknowledgements**

606 This project was funded was by the European Research Council grant
607 “DEMONS” (202844) under the European FP7, and the UK National Cen-
608 tre for Earth Observation “Dynamic Earth and Geohazards” theme (NERC
609 NE/F001487/1: <http://comet.nerc.ac.uk/>). Field support was provided
610 by the NSF under award ANT1142083. ~~TLS~~ [Terrestrial laser scan](#) data were
611 provided by Laura Jones and Jed Frechette. NP wishes to thank Alain Bur-
612 gisser for his helpful comments on the manuscript.

613 **References**

614 Aster, R., Mah, S., Kyle, P., McIntosh, W., Dunbar, N., Johnson, J., Ruiz,
615 M., McNamara, S., 2003. Very long period oscillations of Mount Ere-
616 bus volcano. *Journal of Geophysical Research* 108, 22 PP. URL: [http:
617 //www.agu.org/journals/ABS/2003/2002JB002101.shtml](http://www.agu.org/journals/ABS/2003/2002JB002101.shtml), doi:200310.
618 1029/2002JB002101.

619 Boichu, M., Oppenheimer, C., Tsanev, V., Kyle, P.R., 2010. High
620 temporal resolution SO₂ flux measurements at Erebus volcano,
621 Antarctica. *Journal of Volcanology and Geothermal Research*
622 190, 325336. URL: [http://www.sciencedirect.com/science/
623 article/B6VCS-4XVK3X7-2/2/5becf55734379e128652e28c05da2702](http://www.sciencedirect.com/science/article/B6VCS-4XVK3X7-2/2/5becf55734379e128652e28c05da2702),
624 doi:10.1016/j.jvolgeores.2009.11.020.

625 Bouche, E., Vergnolle, S., Staudacher, T., Nercessian, A., Delmont, J.C.,
626 Frogneux, M., Cartault, F., Le Pichon, A., 2010. The role of large
627 bubbles detected from acoustic measurements on the dynamics of Erta
628 'Ale lava lake (Ethiopia). *Earth and Planetary Science Letters* 295,
629 37–48. URL: [http://www.sciencedirect.com/science/article/pii/
630 S0012821X10001913](http://www.sciencedirect.com/science/article/pii/S0012821X10001913), doi:10.1016/j.epsl.2010.03.020.

631 Bradski, G., 2000. The OpenCV Library. *Dr. Dobb's Journal of Software*
632 *Tools* 25, 120, 122125. URL: [http://www.ddj.com/ftp/2000/2000_11/
633 opencv.txt](http://www.ddj.com/ftp/2000/2000_11/opencv.txt).

634 Bradski, G., Kaehler, A., 2008. *Learning OpenCV: Computer Vision with*
635 *the OpenCV Library*. 1st ed., O'Reilly Media.

- 636 Burgisser, A., Oppenheimer, C., Alletti, M., Kyle, P.R., Scaillet, B., Car-
637 roll, M.R., 2012. Backward tracking of gas chemistry measurements
638 at Erebus volcano. *Geochemistry, Geophysics, Geosystems* 13, n/an/a.
639 URL: [http://onlinelibrary.wiley.com/doi/10.1029/2012GC004243/](http://onlinelibrary.wiley.com/doi/10.1029/2012GC004243/abstract)
640 abstract, doi:10.1029/2012GC004243.
- 641 De Lauro, E., De Martino, S., Falanga, M., Palo, M., 2009. Modelling the
642 macroscopic behavior of Strombolian explosions at Erebus volcano. *Physics*
643 *of the Earth and Planetary Interiors* , 174–186doi:10.1016/j.pepi.2009.
644 05.003.
- 645 Dibble, R., Kyle, P., Rowe, C., 2008. Video and seismic ob-
646 servations of Strombolian eruptions at Erebus volcano, Antarc-
647 tica. *Journal of Volcanology and Geothermal Research* 177,
648 619–634. URL: [http://www.sciencedirect.com/science/](http://www.sciencedirect.com/science/article/B6VCS-4T4J84N-2/2/76386fd18269d42b50f8d4134b25d897)
649 [article/B6VCS-4T4J84N-2/2/76386fd18269d42b50f8d4134b25d897,](http://www.sciencedirect.com/science/article/B6VCS-4T4J84N-2/2/76386fd18269d42b50f8d4134b25d897)
650 doi:10.1016/j.jvolgeores.2008.07.020.
- 651 Divoux, T., Bertin, E., Vidal, V., Gminard, J.C., 2009. Intermittent out-
652 gassing through a non-Newtonian fluid. *Physical Review E* 79, 56204.
- 653 Francis, P., Oppenheimer, C., Stevenson, D., 1993. Endogenous growth of
654 persistently active volcanoes. *Nature* 366, 554–557. URL: [http://dx.](http://dx.doi.org/10.1038/366554a0)
655 [doi.org/10.1038/366554a0](http://dx.doi.org/10.1038/366554a0), doi:10.1038/366554a0.
- 656 Gerst, A., Hort, M., Aster, R.C., Johnson, J.B., Kyle, P.R., 2013. The first
657 second of volcanic eruptions from the Erebus volcano lava lake, Antarctica -
658 energies, pressures, seismology, and infrasound. *Journal of Geophysical Re-*

659 search: Solid Earth 118, 33183340. URL: <http://onlinelibrary.wiley.com/doi/10.1002/jgrb.50234/abstract>, doi:10.1002/jgrb.50234.

660

661 Giggenbach, W.F., Kyle, P.R., Lyon, G.L., 1973. Present volcanic activity
662 on Mount Erebus, Ross Island, Antarctica. *Geology* 1, 135–136. URL:
663 <http://geology.gsapubs.org/cgi/content/abstract/1/3/135>.

664 Hegger, R., Kantz, H., 1999. Improved false nearest neighbor method to
665 detect determinism in time series data. *Physical Review E* 60, 4970–
666 4973. URL: <http://link.aps.org/doi/10.1103/PhysRevE.60.4970>,
667 doi:10.1103/PhysRevE.60.4970.

668 Hegger, R., Kantz, H., Schreiber, T., 1998. Practical implementation of
669 nonlinear time series methods: The TISEAN package. arXiv e-print
670 [chao-dyn/9810005](http://arxiv.org/abs/chao-dyn/9810005). URL: <http://arxiv.org/abs/chao-dyn/9810005>.
671 *CHAOS* 9 (1999) 413.

672 Huppert, H.E., Hallworth, M.A., 2007. Bi-directional flows in
673 constrained systems. *Journal of Fluid Mechanics* 578, 95–112.
674 URL: [http://journals.cambridge.org/action/displayAbstract?](http://journals.cambridge.org/action/displayAbstract?fromPage=online&aid=992960)
675 [fromPage=online&aid=992960](http://journals.cambridge.org/action/displayAbstract?fromPage=online&aid=992960), doi:10.1017/S0022112007004661.

676 Jones, E., Oliphant, T., Peterson, P., 2001. SciPy: open source scientific
677 tools for Python. URL: <http://www.scipy.org/>.

678 Jones, K.R., Johnson, J.B., Aster, R., Kyle, P.R., McIntosh, W., 2008.
679 Infrasonic tracking of large bubble bursts and ash venting at Erebus
680 volcano, Antarctica. *Journal of Volcanology and Geothermal Re-*
681 *search* 177, 661–672. URL: <http://www.sciencedirect.com/science/>

682 article/B6VCS-4RXJYNV-1/2/6c7b8740060985aed604c2bb0bee1efc,
683 doi:10.1016/j.jvolgeores.2008.02.001.

684 Kantz, H., Schreiber, T., 2003. Nonlinear Time Series Analysis. 2nd ed.,
685 Cambridge University Press.

686 Kelly, P.J., Kyle, P.R., Dunbar, N.W., Sims, K.W., 2008. Geo-
687 chemistry and mineralogy of the phonolite lava lake, Ere-
688 bus volcano, Antarctica: 1972-2004 and comparison with older
689 lavas. Journal of Volcanology and Geothermal Research 177,
690 589–605. URL: [http://www.sciencedirect.com/science/
691 article/B6VCS-4RH94TM-3/2/d8a04cd37850676dcf20569d1e3f7958](http://www.sciencedirect.com/science/article/B6VCS-4RH94TM-3/2/d8a04cd37850676dcf20569d1e3f7958),
692 doi:10.1016/j.jvolgeores.2007.11.025.

693 Kennel, M.B., Brown, R., Abarbanel, H.D.I., 1992. Determining embedding
694 dimension for phase-space reconstruction using a geometrical construction.
695 Physical Review A 45, 3403–3411. URL: [http://link.aps.org/doi/10.
696 1103/PhysRevA.45.3403](http://link.aps.org/doi/10.1103/PhysRevA.45.3403), doi:10.1103/PhysRevA.45.3403.

697 Kingsbury, N., 2001. Complex wavelets for shift invariant analysis and
698 filtering of signals. Applied and Computational Harmonic Analysis
699 10, 234253. URL: [http://www.sciencedirect.com/science/article/
700 B6WB3-45BT4JT-X/2/e88b2a92c22b0e1ae0475e7399b0f45f](http://www.sciencedirect.com/science/article/B6WB3-45BT4JT-X/2/e88b2a92c22b0e1ae0475e7399b0f45f), doi:DOI:10.
701 1006/acha.2000.0343.

702 Knox, H., 2012. Eruptive characteristics and glacial earthquake investigation
703 on Erebus volcano, Antarctica. Ph.D. thesis. New Mexico Institute of Min-

704 ing and Technology. URL: [http://www.ees.nmt.edu/outside/alumni/](http://www.ees.nmt.edu/outside/alumni/thesis.php)
705 [thesis.php](http://www.ees.nmt.edu/outside/alumni/thesis.php).

706 Kyle, P.R., Meeker, K., Finnegan, D., 1990. Emission rates of sulfur
707 dioxide, trace gases and metals from Mount Erebus, Antarctica. *Geo-*
708 *physical Research Letters* 17, PP. 2125–2128. URL: [http://www.agu.](http://www.agu.org/pubs/crossref/1990/GL017i012p02125.shtml)
709 [org/pubs/crossref/1990/GL017i012p02125.shtml](http://www.agu.org/pubs/crossref/1990/GL017i012p02125.shtml), doi:199010.1029/
710 GL017i012p02125.

711 Magarey, J., Kingsbury, N., 1998. Motion estimation using a complex-valued
712 wavelet transform. *Signal Processing, IEEE Transactions on* 46, 10691084.
713 doi:10.1109/78.668557.

714 Molina, I., Burgisser, A., Oppenheimer, C., 2012. Numerical simulations
715 of convection in crystal-bearing magmas: A case study of the magmatic
716 system at Erebus, Antarctica. *Journal of Geophysical Research: Solid*
717 *Earth* 117, n/an/a. URL: [http://onlinelibrary.wiley.com/doi/10.](http://onlinelibrary.wiley.com/doi/10.1029/2011JB008760/abstract)
718 [1029/2011JB008760/abstract](http://onlinelibrary.wiley.com/doi/10.1029/2011JB008760/abstract), doi:10.1029/2011JB008760.

719 Moussallam, Y., Oppenheimer, C., Aiuppa, A., Giudice, G., Moussal-
720 lam, M., Kyle, P., 2012. Hydrogen emissions from Erebus volcano,
721 Antarctica. *Bulletin of Volcanology* 74, 2109–2120. URL: [http://link.](http://link.springer.com/content/pdf/10.1007/s00445-012-0649-2.pdf)
722 [springer.com/content/pdf/10.1007/s00445-012-0649-2.pdf](http://link.springer.com/content/pdf/10.1007/s00445-012-0649-2.pdf),
723 doi:10.1007/s00445-012-0649-2.

724 Oppenheimer, C., Lomakina, A.S., Kyle, P.R., Kingsbury, N.G.,
725 Boichu, M., 2009. Pulsatory magma supply to a phonolite lava
726 lake. *Earth and Planetary Science Letters* 284, 392398. URL:

727 [http://www.sciencedirect.com/science/article/B6V61-4WH0JVH-1/](http://www.sciencedirect.com/science/article/B6V61-4WH0JVH-1/2/9bfe0fa47d44d452b045397b50b40d01)
728 [2/9bfe0fa47d44d452b045397b50b40d01](http://www.sciencedirect.com/science/article/B6V61-4WH0JVH-1/2/9bfe0fa47d44d452b045397b50b40d01), doi:10.1016/j.epsl.2009.04.
729 043.

730 Oppenheimer, C., McGonigle, A.J.S., Allard, P., Wooster, M.J., Tsanev, V.,
731 2004. Sulfur, heat, and magma budget of Erta 'Ale lava lake, Ethiopia.
732 *Geology* 32, 509–512. URL: [http://geology.gsapubs.org/content/32/](http://geology.gsapubs.org/content/32/6/509)
733 [6/509](http://geology.gsapubs.org/content/32/6/509), doi:10.1130/G20281.1.

734 Oppenheimer, C., Moretti, R., Kyle, P.R., Eschenbacher, A., Lowenstern,
735 J.B., Hervig, R.L., Dunbar, N.W., 2011. Mantle to surface degassing of al-
736 kalic magmas at Erebus volcano, Antarctica. *Earth and Planetary Science*
737 *Letters* 306, 261–271. URL: [http://www.sciencedirect.com/science/](http://www.sciencedirect.com/science/article/pii/S0012821X11002111)
738 [article/pii/S0012821X11002111](http://www.sciencedirect.com/science/article/pii/S0012821X11002111), doi:10.1016/j.epsl.2011.04.005.

739 Orr, T.R., Rea, J.C., 2012. Time-lapse camera observations of gas pis-
740 ton activity at Pu'u 'Ō'ō, Kīlauea volcano, Hawai'i. *Bulletin of Vol-*
741 *canology* 74, 2353–2362. URL: [http://link.springer.com/10.1007/](http://link.springer.com/10.1007/s00445-012-0667-0)
742 [s00445-012-0667-0](http://link.springer.com/10.1007/s00445-012-0667-0), doi:10.1007/s00445-012-0667-0.

743 Patrick, M.R., Orr, T., Wilson, D., Dow, D., Freeman, R., 2011. Cyclic spat-
744 tering, seismic tremor, and surface fluctuation within a perched lava chan-
745 nel, Kīlauea Volcano. *Bulletin of Volcanology* 73, 639–653. URL: [http://link.springer.com/article/10.1007/](http://link.springer.com/article/10.1007/s00445-010-0431-2)
746 [s00445-010-0431-2](http://link.springer.com/article/10.1007/s00445-010-0431-2), doi:10.
747 [1007/s00445-010-0431-2](http://link.springer.com/article/10.1007/s00445-010-0431-2).

748 Peters, N., Oppenheimer, C., Kyle, P., 2014. Autonomous thermal cam-
749 era system for monitoring the active lava lake at Erebus volcano, Antarc-

750 tica. *Geoscientific Instrumentation, Methods and Data Systems* 3, 13–
751 20. URL: [http://www.geosci-instrum-method-data-syst.net/3/13/](http://www.geosci-instrum-method-data-syst.net/3/13/2014/gi-3-13-2014.html)
752 [2014/gi-3-13-2014.html](http://www.geosci-instrum-method-data-syst.net/3/13/2014/gi-3-13-2014.html), doi:10.5194/gi-3-13-2014.

753 Polikar, R., 2010. The Wavelet Tutorial. URL: [http://users.rowan.edu/](http://users.rowan.edu/~polikar/WAVELETS/WTtutorial.html)
754 [~polikar/WAVELETS/WTtutorial.html](http://users.rowan.edu/~polikar/WAVELETS/WTtutorial.html).

755 Richter, M., Schreiber, T., 1998. Phase space embedding of electrocardio-
756 grams. *Physical Review E* 58, 6392–6398. URL: [http://link.aps.org/](http://link.aps.org/doi/10.1103/PhysRevE.58.6392)
757 [doi/10.1103/PhysRevE.58.6392](http://link.aps.org/doi/10.1103/PhysRevE.58.6392), doi:10.1103/PhysRevE.58.6392.

758 Schreiber, T., Schmitz, A., 1999. Surrogate time series. arXiv e-print chao-
759 dyn/9909037. URL: <http://arxiv.org/abs/chao-dyn/9909037>. *physica*
760 *D* 142 (2000) 346-382.

761 Sweeney, D., Kyle, P.R., Oppenheimer, C., 2008. Sulfur diox-
762 ide emissions and degassing behavior of Erebus volcano, Antarc-
763 tica. *Journal of Volcanology and Geothermal Research* 177,
764 725–733. URL: [http://www.sciencedirect.com/science/](http://www.sciencedirect.com/science/article/B6VCS-4S1C8B5-2/2/4950721356ddb16e9b4e4f054b9efc81)
765 [article/B6VCS-4S1C8B5-2/2/4950721356ddb16e9b4e4f054b9efc81](http://www.sciencedirect.com/science/article/B6VCS-4S1C8B5-2/2/4950721356ddb16e9b4e4f054b9efc81),
766 doi:10.1016/j.jvolgeores.2008.01.024.

767 Tilling, R.I., 1987. Fluctuations in surface height of active lava
768 lakes during 1972-1974 Mauna Ulu Eruption, Kilauea Volcano,
769 Hawaii. *Journal of Geophysical Research: Solid Earth* 92,
770 1372113730. URL: [http://onlinelibrary.wiley.com/doi/10.1029/](http://onlinelibrary.wiley.com/doi/10.1029/JB092iB13p13721/abstract)
771 [JB092iB13p13721/abstract](http://onlinelibrary.wiley.com/doi/10.1029/JB092iB13p13721/abstract), doi:10.1029/JB092iB13p13721.

- 772 Witham, F., Llewelin, E.W., 2006. Stability of lava lakes. *Journal of*
773 *Volcanology and Geothermal Research* 158, 321–332. URL:
774 [http://www.sciencedirect.com/science/article/B6VCS-4M04J4P-1/](http://www.sciencedirect.com/science/article/B6VCS-4M04J4P-1/2/be09707e9f17ab20c2b06bb0929b5790)
775 [2/be09707e9f17ab20c2b06bb0929b5790](http://www.sciencedirect.com/science/article/B6VCS-4M04J4P-1/2/be09707e9f17ab20c2b06bb0929b5790), doi:10.1016/j.jvolgeores.
776 2006.07.004.
- 777 Witham, F., Woods, A.W., Gladstone, C., 2006. An analogue exper-
778 imental model of depth fluctuations in lava lakes. *Bulletin of Vol-*
779 *canology* 69, 51–56. URL: [http://www.springerlink.com/content/](http://www.springerlink.com/content/130v288277011h1w/)
780 [130v288277011h1w/](http://www.springerlink.com/content/130v288277011h1w/), doi:10.1007/s00445-006-0055-8.
- 781 Wright, R., Pilger, E., 2008. Satellite observations reveal little
782 inter-annual variability in the radiant flux from the Mount Ere-
783 bus lava lake. *Journal of Volcanology and Geothermal Research*
784 177, 687–694. URL: [http://www.sciencedirect.com/science/](http://www.sciencedirect.com/science/article/B6VCS-4S39MN5-3/2/5078fc4e6bb50a65858e4b8d550d4593)
785 [article/B6VCS-4S39MN5-3/2/5078fc4e6bb50a65858e4b8d550d4593](http://www.sciencedirect.com/science/article/B6VCS-4S39MN5-3/2/5078fc4e6bb50a65858e4b8d550d4593),
786 doi:10.1016/j.jvolgeores.2008.03.005.
- 787 Zandomeneghi, D., Aster, R., Kyle, P., Barclay, A., Chaput, J.,
788 Knox, H., 2013. Internal structure of Erebus volcano, Antarc-
789 tica imaged by high-resolution active-source seismic tomography and
790 coda interferometry. *Journal of Geophysical Research: Solid Earth*
791 118, 10671078. URL: [http://onlinelibrary.wiley.com/doi/10.1002/](http://onlinelibrary.wiley.com/doi/10.1002/jgrb.50073/abstract)
792 [jgrb.50073/abstract](http://onlinelibrary.wiley.com/doi/10.1002/jgrb.50073/abstract), doi:10.1002/jgrb.50073.

793 **Appendix A. Phase Space Reconstruction of Mean Speed Time**
794 **Series**

795 A clear description of the method of delays for phase space reconstruction
796 is given by Kantz and Schreiber (2003) and also by Richter and Schreiber
797 (1998). We will therefore not attempt to describe the technique in any detail
798 here, instead we give the specifics of how the parameters required for delay
799 reconstruction were calculated for our time series. Essentially, phase space
800 reconstruction of a time series involves mapping each sample in the series to
801 a vector in phase space. For a scalar time series x_1, x_2, x_3, \dots the method
802 of delays can be used to calculate the corresponding phase space vectors
803 $\mathbf{x}_n = (x_n, x_{n-l}, x_{n-2l}, \dots, x_{n-(d-1)l})$ where l is known as the lag, and d is
804 the embedding dimension. [Figure A.10 shows an example of phase space](#)
805 [reconstruction using the method of delays with an embedding dimension of](#)
806 [2, and demonstrates how points in the time series are mapped into phase](#)
807 [space.](#)

808 Careful selection of both the lag and the embedding dimension are paramount
809 to obtaining an effective phase space reconstruction of the original time series.
810 Estimation of a suitable lag for our data was performed using two different
811 techniques. The first was to calculate the autocorrelation function of the
812 time series. The time required for the autocorrelation function to decay by
813 a factor of e is stated as being a reasonable estimate for the lag (Kantz and
814 Schreiber, 2003). For our data, this gave a lag of 142 s. A second technique
815 for lag estimation, also described by Kantz and Schreiber (2003), is to find
816 the minimum of the mutual information of the time series. We calculated the
817 mutual information of our time series using the TISEAN software package

818 (Hegger et al., 1998), and found the minimum to be at 200 s. We repeated our
819 bubble event analysis for several different values of lag between these two es-
820 timates and found no appreciable difference in the results. ~~For no particular~~
821 ~~reason, the~~ The results presented in this paper are from the analysis using a
822 lag of 150 s.

823 To determine a good embedding dimension, we followed the approach
824 proposed by Hegger and Kantz (1999), in which the false nearest neighbour
825 method (Kennel et al., 1992) is combined with surrogate data tests. The false
826 nearest neighbour method compares the ratio of distances between points and
827 their nearest neighbours between an embedding dimension of n and $n+1$. If
828 the ratio is greater than a threshold (s), the points are said to be “false
829 neighbours”. A high percentage of false nearest neighbours is indicative of
830 too low a choice for the embedding dimension. The TISEAN software pack-
831 age was used both for the calculation of false nearest neighbours and for the
832 creation of surrogate data (Schreiber and Schmitz, 1999). Figure A.11 shows
833 the calculated percentage of false nearest neighbours for different embedding
834 dimensions and thresholds. There is a clear difference in behaviour between
835 the real data and the surrogate data. This indicates that the loss of false
836 neighbours as we move to higher embedding dimensions is not simply due
837 to linear correlations in the data. Furthermore, we can see that for an em-
838 bedding dimension of 4, the percentage of false nearest neighbours falls away
839 very rapidly for low threshold values. We therefore used 4 as our embedding
840 dimension when performing the phase space reconstruction.

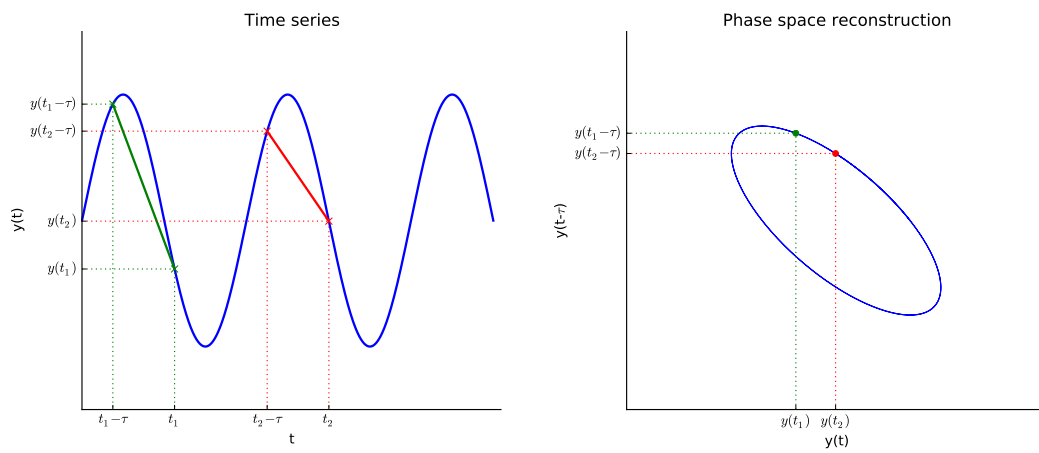


Figure A.10: Phase space reconstruction of a simple time series using the method of delays. The original time series is shown in the left hand plot and the phase space reconstruction using a lag of τ and an embedding dimension of 2 is shown in the right hand plot. Samples from the time series (e.g. t_1 and t_2) are mapped to phase space by plotting them against the value of the time series one lag prior to their sample time.

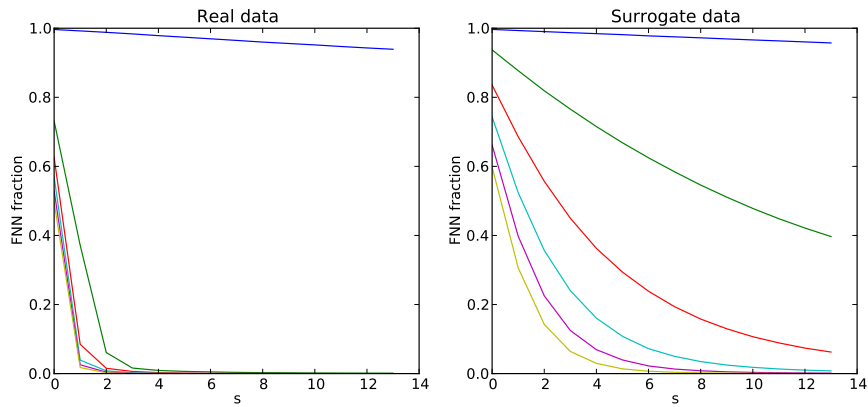


Figure A.11: The fraction of false nearest neighbours (FNN) against the threshold value for embedding dimensions from 1 to 6 (top to bottom) and a lag of 150 s, for both the real data (left hand plot) and a surrogate data series (right hand plot). The difference between the real and surrogate data shows that the reduction in FNN as we increase the embedding dimension is not simply due to linear correlations in the data. For an embedding dimension of 4, the FNN fraction reduces very quickly for small threshold values and there is little difference in behaviour compared to larger embedding dimensions. We therefore chose 4 as a suitable embedding dimension for our analysis.